Estimation of Piston Surface Temperature During Engine Transient Operation for Emissions Reduction

Zhijia Yang

Department of Aeronautical and Automotive Engineering, Loughborough University, Loughborough LE113TU, UK

Byron Mason[1]

Department of Aeronautical and Automotive Engineering, Loughborough University, Loughborough, Leicestershire LE11 3TU, UK e-mail: b.mason2@lboro.ac.uk

Brian Wooyeol Bae

Department of Aeronautical and Automotive Engineering, Loughborough University, Loughborough LE113TU, UK

Fabrizio Bonatesta

School of Engineering, Computing and Mathematics, Oxford-Brookes University, Oxford, Oxfordshire OX33 1HX, UK

Edward Winward

Department of Aeronautical and Automotive Engineering, Loughborough University, Loughborough, Leicestershire LE11 3TU, UK

Richard Burke

Department of Mechanical Engineering, University of Bath, Bath BA2 7AYd, UK

Edward Chappell

Department of Mechanical Engineering, University of Bath, Bath BA2 7AY, UK

[1]Corresponding author.

Abstract

Piston surface temperature is an important factor in the reduction of harmful emissions in modern gasoline direct injection (GDI) engines. In transient operation, the piston surface temperature can change rapidly, increasing the risk of fuel puddling. The prediction of the piston surface temperature can provide the means to significantly improve multiple-pulse fuel injection control strategies through the avoidance of fuel puddling. It could also be used to intelligently control the piston cooling jet (PCJ), which is common in modern engines. Considerable research has been undertaken to identify generalized engine heat transfer correlations and to predict piston and cylinder wall surface temperatures during operation. Most of these correlations require in-cylinder combustion pressure as an input, as well as the identification of numerous model parameters. These requirements render such an approach impractical. In this study, the authors have developed a thermodynamic model of piston surface temperature based on the global energy balance (GEB) methodology, which includes the effect of PCJ activation. The advantages are a simple structure and no requirement for in-cylinder pressure data, and only limited experimental tests are needed for model parameter identification. Moreover, the proposed model works well during engine transient operation, with maximum average error of 6.68% during rapid transients. A detailed identification procedure is given. This and the model performance have been demonstrated using experimental piston crown surface temperature data from a prototype 1-liter 3-cylinder turbocharged GDI engine, operated in both engine steady-state and transient conditions with an oil jet used for piston cooling turned both on and off.

Keywords: combustion, experimental, heat transfer, internal combustion engines, modeling, piston surface temperature

1 Introduction

It is well recognized that the performance of advanced combustion modes such as homogeneous charge compression ignition (HCCI), low temperature diffusion combustion, and premixed charge compression ignition is very sensitive to cylinder wall temperature [1]. An accurate estimate of this temperature can help improve combustion stability control in advanced combustion modes [2].

1.1 Piston Temperature Impact on Engine Emissions.

For GDI engines, particulate emission (both mass PM, and number PN) is often the foremost concern due to its harmful impact [3]. This is reflected by strict limits imposed by the latest regulatory frameworks [4]. In modern, smaller GDI engine cylinders, the use of high pressure fuel injection inevitably leads to liquid-spray wall impingement and in turn to the formation of liquid film. During the combustion process, any retained film traces may cause locally rich diffusive combustion (pool fire) and high PM/PN emissions. Piston surface temperature exerts an important influence on both liquid film deposition and film evaporation. Relatively low piston and wall temperatures cause increasing particulate emissions [5,6] as well as a deterioration of the brake specific fuel consumption (BSFC) (i.e., fuel economy) by wasting fuel energy. These phenomena are strongly

exacerbated in cold start conditions [7,8].

1.2 Piston Cooling Jet.

Modern internal combustion engines (ICE) are equipped with a PCJ system, which can protect the piston crown (also referred to as the piston head) from overheating. When the PCJ is switched on, an oil jet is squirted underneath the piston crown at high relative velocity to cool the piston [9,10]. Najafabadi et al. show that the PCJ is able to reduce CO, NO_x, and HC emissions between 3% and 10% across the engine speed-load range [11]. Although evidence can be indirectly drawn from a number of publications, for example, [12], no papers could be found that directly examine the effects of PCJ cooling strategies on particulate emissions. Studies on the PCJ system can be found in the literature; however, the majority of them are based on complex three-dimensional computational fluid dynamics (CFD) simulation [10,13,14]. Zero-dimensional heat transfer correlation models for PCJ operation developed and validated on the basis of experimental data can be found in Refs. [9,15].

1.3 Piston Temperature Modeling.

Biagiotti et al. [5] propose a state-of-the-art CFD approach to model the liquid film dynamics in GDI engines. This study highlights the importance of realistic inputs for piston, cylinder head, and cylinder wall temperatures to enable accurate liquid film and, in turn, particulate formation predictions. Surface temperatures are shown not to vary significantly during the mixture preparation phase (injection to spark) [12,16] and therefore homogeneous and constant temperature boundary conditions are deemed sufficient for the analysis. The simplified piston temperature model proposed in the present paper can also be coupled with sophisticated CFD simulations of the engine cycle for diagnostic or control strategy optimization.

Using more traditional, single-pulse fuel injection control strategies, it is not always possible to reduce BSFC without an excessive compromise on particulate emissions. However, there is evidence that PM/PN emissions and BSFC in GDI engines can be simultaneously improved by the adoption of Multiple-pulse Injection (MI) strategy [17,18]. There are multiple benefits of an MI strategy. MI can be used to realize a homogeneous air–fuel gas-phase mixture while minimizing the impact between liquid spray and walls, to reduce particulate formation [17], and/or to realize a stratified lean mixture during the compression stroke to also reduce BSFC [18]. To achieve the benefits of MI, a practical means of estimating particulate matter formation and, prior to that, piston crown temperature should be in place, for example, using mean value engine models (MVEMs). The development of an accurate model of piston crown temperature is therefore the first step to control PN and BSFC via an MI strategy. Furthermore, the information can be used to optimize the operation of PCJ and set the piston temperature within a desired range.

A popular model of instantaneous cylinder heat transfer was developed by Woschni, which is well known as the Woschni heat transfer correlation [19]. This model was subsequently modified by Chang et al. for application in a multicylinder HCCI engine and the estimated wall temperature was used in modulating residual

gas fraction for improved control during transient operation [20]. The authors in Ref. [1] formed an unknown input observer based on the instantaneous Woschni heat transfer correlation to predict cylinder wall temperature from intake valve close to start of injection in a medium-duty diesel engine. The model was used to support active fueling control, particularly during cold-start and transient operations. The fitting of these heat transfer model parameters is normally based on engine steady-state data, and this type of model needs in-cylinder pressure as an input. A system identification (SI)-based linear three-order dynamic state space model for chamber wall temperature of a HCCI engine was developed in Ref. [2]. The model input is the online measured indicated mean effective pressure (IMEP) signal; the engine data used for model development include IMEP and wall temperature, measured during a cycle perturbed by a pseudo-random binary sequence signal at constant engine speed.

Several recent examples of engine wall temperature modeling can be found in Refs. [21,22], and related experimental work is discussed in Ref. [23]. In Ref. [21], a zero-dimensional single-zone thermodynamic engine model was coupled with a 1D transient heat transfer model. In Ref. [22], this earlier model framework was augmented with heat release computed using CFD. These models were used to investigate thermal barrier coatings in engines. To evaluate the model performance, the authors used measured cylinder pressure, gross-indicated mean effective pressure, and the air mass flowrate as surrogates for the in-cylinder wall temperature. This is due to the significant challenges of fast temperature measurements of the in-cylinder surfaces.

1.4 Global Energy Balance.

Global energy balance has been demonstrated to be a very effective approach for the development of zero-dimensional heat transfer correlations for ICEs [24,25]. A comprehensive experimental study of heat transfer within engine cylinders is presented in Ref. [26]. An overall average engine heat transfer model was developed based on experimental data from a wide range of engine specifications: two and four stroke engines, diesel and gasoline engines, different compression ratios, different engine capacities, and different spark ignition setting [26]. The proposed model only requires gas thermal properties, engine speed, or gas mass flowrate. A recent review of internal combustion engine heat transfer and wall temperature modeling can be found in Ref. [27].

1.5 Research Approach.

In the present study, the authors have developed a thermodynamic model of piston surface temperature based on the GEB methodology and the overall heat transfer correlation structure proposed in Ref. [26]. Importantly, the model introduces a specific, parallel heat transfer path when the PCJ is activated. The thermodynamics are modeled using a lumped piston mass. The advantage of this type of model is that it is simple in structure, does not need in-cylinder pressure data, requires only limited test data for parameter identification, and works well in engine transient operation.

A detailed account of the identification procedure for the model parameters is given in this paper using experimental piston crown surface temperature data from a prototype 1-liter 3-cylinder Turbocharged Gasoline

Direct Injection (T-GDI) engine, operated under both steady-state and transient conditions, coupled with PCJ on and off states.

The paper is organized as follows: Section 2 introduces the dynamic piston surface temperature model. Section 3 provides details of the model identification procedure. Section 4 describes the experimental setup used for collecting the engine data for both model parameter identification and model validation. Section 5 presents results of the model performance for both steady-state and transient operating conditions. Conclusions are drawn in Sec. 6. The Appendix presents details of the polynomial regression models used to estimate the gas properties required in the piston temperature model.

2 A Thermodynamic Model for Piston Surface Temperature

The dynamic model for piston surface temperature is based on the GEB principle, which means that modeling of complex combustion processes for engine transient operation conditions is not required. It also uses the overall heat transfer correlation structure proposed in Ref. [26], which greatly reduces the model complexity.

2.1 Model Structure.

The model structure is shown in Fig. 1 in the form of a thermal resistance network. As the heat transfer correlation is only considered at an overall level, this model structure represents the overall heat transfer performance for multicylinder engines. It is similar to the concept to a MVEM.

Fig. 1 Model structure for piston surface temperature dynamic model
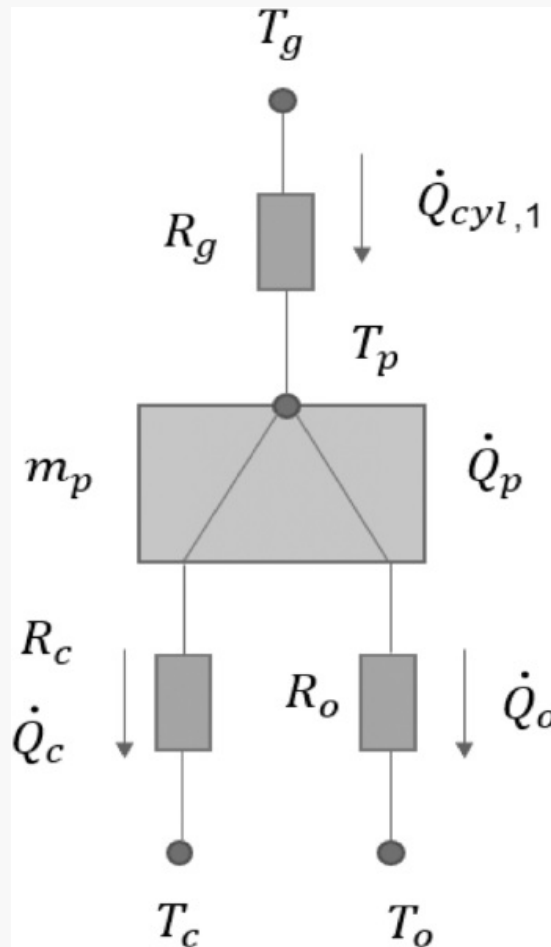
There are only four temperature nodes, which are T_g, T_c, T_o, and T_p for combustion gas temperature, coolant temperature, oil jet temperature, and piston surface temperature, respectively. T_c and T_o are two inputs to the model. T_g is not explicitly needed in the model because the heat flowrate $\dot{Q}_{cyl,1}$ from hot combustion gas to piston surface can be estimated using the engine external GEB approach. This vastly simplifies both development and application of the model.

There are only three lumped thermal resistances in this model structure; they are R_g for modeling the heat transfer path from the combustion gas to the piston surface; R_c for the path between piston surface and coolant flow; and R_o for the path between piston surface and PCJ oil flow within the piston crown. Similar to T_g, there is no need to estimate the thermal resistance R_g explicitly. R_c and R_o can be identified using the overall

heat transfer correlation from steady-state engine experimental data when PCJ is off. When T_p, T_c, and T_o are known, R_c and R_o can be identified using experimental steady-state data.

$\dot{Q}_c$ and $\dot{Q}_o$ are the heat transfer rates from piston surface to coolant and from piston surface to PCJ oil when PCJ is on, respectively. $\dot{Q}_p$ is the heat transfer rate from combustion gas to the piston crown, which is the main cause of the piston temperature thermodynamics. Finally, m_p is the lumped mass of the piston crown of all cylinders associated with the thermodynamic behavior of the piston surface temperature. It was estimated using experimental data in this work.

2.2 Model Equations.

The model consists of three parts which are the following: (1) External GEB for estimating $\dot{Q}_{cyl}$, (2) Energy conservation equations for the thermal resistance network depicted in Fig. 1, and (3) Equations for modeling the two thermal resistance R_c and R_o, which are based on an overall heat transfer correlation approach [26].

2.2.1 Model Part 1/3: External Global Energy Balance.

The heat flow within the engine and between engine and environment is complicated; however, it can be described using a simple energy balance, which includes only four terms

$$\dot{Q}_{in} = P_{out} + P_{mechloss} + \dot{Q}_{cyl,1} + \dot{Q}_{cyl,2} + \dot{Q}_{exh} \tag{1}$$

where $\dot{Q}_{in}$ is the heat input from fuel, P_{out} is the engine mechanical brake power output, $P_{mechloss}$ is the friction and pumping losses, and $\dot{Q}_{cyl,1}$ is the heat flow from combustion gas to the coolant and the PCJ oil flows (when PCJ is activated). The PCJ oil often enters a small hole on the underside of the piston and flows around a channel inside the piston then exiting, thus removing heat from the piston. $\dot{Q}_{exh}$ is the heat transfer from the exhaust gas stream. To simplify the model, $\dot{Q}_{cyl,2}$, the heat transfer from combustion gas to coolant and to engine environment via ports and extra parts (other than piston crown) together with $P_{mechloss}$ is modeled as proportional to the heat input from the fuel, that is

$$\dot{Q}_{cyl,2} + P_{mechloss} = r\dot{Q}_{in} \tag{2}$$

where $0 < r < 1$ and varies with engine operating point. It was identified as one integrated model parameter with combustion efficiency for each tested engine operating point.

The mechanical brake power output can be estimated as

$$P_{out} = \frac{2\pi N_e T_e}{60} \tag{3}$$

where N_e is engine rotational speed in units of revolutions/minute (rpm), and T_e is engine brake torque in units of newton/meter (Nm). The heat carried by the exhaust gas can be estimated using

$$\dot{Q}_{\text{exh}} = (\dot{m}_a + \dot{m}_f)C_{p,g}(T_{\text{exh}} - T_{\text{in}}) \tag{4}$$

where T_{exh} and T_{in} are exhaust gas temperature and intake manifold temperature, respectively. $\dot{m}_a$ and $\dot{m}_f$ are intake air mass flowrate and fuel mass flowrate. A regression equation has been fitted for $C_{p,g}$ using data reported in literature, see Appendix A4.

The heat input from fuel can be calculated as

$$\dot{Q}_{in} = \eta_c \dot{m}_f Q_{\text{LHV}} \tag{5}$$

where Q_{LHV} is the Lower Heating Value of the gasoline fuel. A constant value of 43.4 MJ/kg was used in this study. η_c is the engine combustion efficiency, which varies as a function of the operating point. It can be written as $\eta_c(N_e, T_e)$. This was identified as a 2D look-up table using the steady-state experimental data when PCJ is off.

By rearranging Eq. (2), the heat flow from combustion gas to coolant via the piston crown can be estimated as

$$\begin{aligned} \dot{Q}_{\text{cyl},1} &= \dot{Q}_{in} - \dot{Q}_{\text{cyl},2} - P_{\text{out}} - \dot{Q}_{\text{exh}} \\ &= (1 - r)\dot{Q}_{in} - P_{\text{out}} - \dot{Q}_{\text{exh}} \end{aligned} \tag{6}$$

Using the right side of Eq. (5) to replace $\dot{Q}_{\text{in}}$, Eq. (6) can be rewritten as

$$\dot{Q}_{\text{cyl},1} = (1 - r)\eta_c \dot{m}_f Q_{\text{LHV}} - P_{\text{out}} - \dot{Q}_{\text{exh}} \tag{7}$$

where the model parameters r and η_c can be grouped together and identified as one item, e.g., $\eta_h = (1 - r)\eta_c$ using experimental data.

2.2.2 Model Part 2/3: Thermal Resistance Network.

There are four equations for the thermal resistance network in Fig. 1.

The energy conservation equation for this network is

$$\dot{Q}_{\text{cyl},1} = \dot{Q}_c + s_{\text{PCJ}}\dot{Q}_o \tag{8}$$

where s_{PCJ} is a flag signal for PCJ on and off, which can assume only two values, 0 when PCJ is off and 1 when PCJ is on.

The heat flowrate within the mass of the piston crown can be modeled as

$$\dot{Q}_p = m_p C_p \frac{dT_p}{dt} \qquad (9)$$

where C_p is the specific heat capacity of the piston crown. A constant value of 1020 (J/kg.K) is used.

The equations for computing $\dot{Q}_c$ and $\dot{Q}_o$ are

$$\dot{Q}_c = R_c(T_p - T_c) \qquad (10)$$

$$\dot{Q}_o = R_o(T_p - T_o) \qquad (11)$$

2.2.3 Model Part 3/3: Thermal Resistance.

The models for R_c and R_o have the form of an overall heat transfer correlation [26], which can be described using three equations. The key correlation discovered by Taylor is the relationship between Nusselt and Reynolds Numbers of the combustion gas, which is

$$\text{Nu} = K\text{Re}^n \qquad (12)$$

Nu is the Nusselt Number (unitless), which is the ratio of convection to conduction of the combustion gas, see Eq. (13). Re is the Reynolds Number (unitless), which can be estimated in two different ways; one using gas mass flowrate, see Eq. (14). The other using mean piston speed, see Eq. (16). K and n are constants.

The Nusselt Number can be expressed as

$$\text{Nu} = \frac{h_{cyl}b}{k_g} \qquad (13)$$

where h_{cyl} is the heat transfer coefficient, with units of $(\text{W/m}^2\text{K})$. b is the characteristic length, which normally refers to the cylinder bore (i.e., diameter). k_g is the gas thermal conductivity with units of $(\text{W/m} \cdot \text{K})$. Since the gas thermal conductivity increases with temperature, a second-order polynomial regression model was developed for k_g, see Appendix A1.

The gas mass flowrate version of the Reynolds Number is given by

$$\text{Re} = \frac{(\dot{m}_a + \dot{m}_f)b}{A_p \mu_g} \qquad (14)$$

where A_p is the cylinder reference area defined in Eq. (15). μ_g is gas dynamic viscosity, its correlation with temperature was found using air dynamic viscosity data found in Ref. [28], see Appendix A2

$$A_p = \frac{\pi b^2}{4} \tag{15}$$

The mean piston speed version of the Reynolds Number is given by

$$\text{Re} = \frac{V_p b}{\nu_g} \tag{16}$$

where V_p is the mean piston speed used as the characteristic gas velocity, defined in Eq. (17). ν_g is the gas kinematic viscosity with units of (m^2/s). A second-order polynomial regression model for ν_g was obtained using air kinematic viscosity data found in Ref. [28], see Appendix A3.

The mean piston speed is calculated as

$$V_p = \frac{2N_e}{60} L \tag{17}$$

where L is engine stroke length.

The mean piston speed version of the Reynolds number was used in this study since the piston drives the movement of the gasses in the closed cylinder. By combining Eqs. (12), (13), (16), and (17), the combustion overall heat transfer coefficient from piston surface to coolant and PCJ oil can be calculated as

$$h_{\text{cyl}} = \frac{K k_g}{b} \left(\frac{2 N_e L b}{60 \nu_g} \right)^n \tag{18}$$

where K is a constant, and n is a constant power index.

The overall heat transfer coefficient for coolant path h_c and PCJ oil path h_o shown in Fig. 1 could be assumed as having the same correlation pattern as that in Eq. (18)

$$h_c = \frac{K_c k_g}{b} \left(\frac{2 N_e L b}{60 \nu_g} \right)^{n_c} \tag{19}$$

$$h_o = \frac{K_o k_g}{b} \left(\frac{2 N_e L b}{60 \nu_g} \right)^{n_o} \tag{20}$$

The constants K and n are chosen to be different for coolant path and PCJ oil jet path; these are K_c, n_c, and K_o, n_o, respectively. They can be identified using engine steady-state experimental data.

Finally, the thermal resistances for the coolant and oil paths can be estimated as

$$R_c = h_c A_p \tag{21}$$

$$R_o = h_o A_p \tag{22}$$

3 Model Parameter Identification

The model parameters that need to be determined are:

(1) 2D look up table for model parameter η_h, function of engine speed and torque: $\eta_h(N_e, T_e)$.

(2) The two constants K_c and n_c for the overall heat transfer coefficient in Eq. (19) for the coolant heat transfer path.

(3) The two constants K_o and n_o for the overall heat transfer coefficient in Eq. (20) for the PCJ oil flow heat transfer path.

(4) The lumped mass of piston crown m_p.

The test data used in this study for the identification of the above are comprised of steady-state data for PCJ off, steady-state data for PCJ on, engine transient data, and a torque ramp at constant engine speed. A total of eleven variables are required, as follows:

(1) Engine speed, N_e

(2) Engine torque, T_e

(3) Intake manifold air mass flow rate, $\dot{m}_a$

(4) Fuel mass flow rate, $\dot{m}_f$

(5) Intake manifold temperature, T_{in}

(6) Exhaust manifold temperature, T_{exh}

(7) Coolant temperature, T_c

(8) Oil gallery temperature, T_o

(9) PCJ on/off flag, s_{PCJ}

(10) Piston surface temperature, T_p

Fast-response thermocouples with diameter of 0.1 mm were used for measuring piston surface temperature T_p and exhaust temperature (EXT) T_{exh}. The slow response of larger diameter thermocouples will give large measurement errors during fast transients, resulting in large errors in the estimation of $\dot{Q}_{cyl,1}$.

The identification procedure for the above model parameters consists of three steps:

Step 1: Use steady-state engine test data with PCJ off to estimate the 2D look up table for $\eta_h = f(N_e, T_e)$. The two constants K_c and n_c for the coolant path overall heat transfer coefficient were set to 20 and 0.75, respectively. They were initially set to the values suggested by Taylor [26], which are 10.5 and 0.75 and further optimized at the outer loop level.

Step 2: Use steady-state engine test data with PCJ on to estimate the two constants K_o and n_o for the overall heat transfer correlation for the PCJ path.

– Step 3: Use torque ramp transient data to identify the lumped piston mass m_p.

In engine steady-state operating conditions with PCJ off, $s_{PCJ} = 0$ in Eq. (8). Equations 1–8, 19, and 21 can be integrated together to form the estimation equation for piston surface temperature

$$\widehat{T}_p = D\left(\eta_h\left(N_e, T_e\right)\dot{m}_f Q_{LHV} - \frac{2\pi N_e T_e}{60}\right)$$
$$- D(\dot{m}_a + \dot{m}_f)C_{p,g}(T_{exh} - T_{in}) + T_c$$

(23)

where $D = [A_p \frac{K_c k_g}{b} G^{n_c}]^{-1}$ and $G = (\frac{2N_e Lb}{60\nu_g})$

The identification of $\eta_h(N_e, T_e)$ can be achieved by solving the following optimization problem:

$$\text{minimize}: \quad J(\eta_c(N_e, T_e)) = \sum_{i=1}^{N_1} (T_p - \widehat{T}_p)^2$$
$$\text{subject to}: \quad 0 < \eta_h(N_e, T_e) < 1$$

(24)

where T_p is the measured piston surface temperature, $\widehat{T}_p$ is computed from Eq. (23), and N_1 is the total number of steady-state data points with PCJ off.

In engine steady-state operating conditions with PCJ on, $s_{PCJ} = 1$ in Eq. (8). The model for piston surface temperature becomes

$$\widehat{T}_p = B\left(\eta_h\left(N_e, T_e\right)\dot{m}_f Q_{LHV} - P_{out} - \dot{Q}_{exh}\right)$$
$$+ B\frac{A_p k_g}{b}[K_c G^{n_c} T_c + K_o G^{n_o} T_o]$$

(25)

where; $B = [\frac{A_p k_g}{b}(K_c G^{n_c} + K_o G^{n_o})]^{-1}$

The identification of the two constant K_o and n_o for the PCJ heat transfer correlation can be obtained by

solving the following optimization problem:

$$\text{minimize}: \quad J(K_o, n_o) = \sum_{i=1}^{N_2} (T_p - \widehat{T}_p)^2$$
$$\text{subject to}: \quad 0 < K_0, 0 < n_o < 1 \tag{26}$$

where T_p is measured piston surface temperature, $\widehat{T}_p$ is computed from Eq. (25), and N_2 is the total number of steady-state data points for PCJ on.

At nonsteady-state operating conditions, $\frac{dT_p}{dt} \neq 0$. Equation (9) can be rewritten in discrete form as follows:

$$\dot{Q}_p(n) = m_p C_p \frac{T_p(n) - T_p(n-1)}{T_s} \tag{27}$$

where T_s is the sample time of the data collection during the experimental testing; n refers to the current value, $n-1$ refers to the previous sample point value. The thermal model of piston surface temperature in transient conditions is written

$$\widehat{T}_p(n) = C(T_s \dot{Q}_{\text{cyl,1}}(n) + T_s R_c(n) T_c(n))$$
$$+C(s_{\text{PCJ}}(n) T_s R_o(n) T_o(n) + m_p C_p \widehat{T}_p(n-1)) \tag{28}$$

where $C = [m_p C_p + T_s R_c(n) + s_{\text{PCJ}}(n) T_s R_o(n)]^{-1}$

The identification of the constant m_p can be obtained by solving the following optimization problem:

$$\text{minimize}: J(m_p) = \sum_{i=1}^{N_3} (T_p(n) - \widehat{T}_p(n))^2 \tag{29}$$

$$\text{subject to}: 0 < m_p \tag{30}$$

where $T_p(n)$ is measured piston surface temperature, $\widehat{T}_p(n)$ is computed from Eq. (28), and N_3 is the total number of sample points within the torque ramp dataset.

4 Experimental Setup and Data Collection

A prototype 1-liter, 3-cylinder T-GDI engine, with a cylinder bore of 79.1 mm, stroke of 82 mm, and compression ratio of 10:1, was setup and fully instrumented in a test cell at the University of Bath, UK. The engine was connected to a 200-kW fully dynamic AC dynamometer test cell with full transient control of engine speed and load through a Sierra CP CADET control system which allows engine speed and torque to be controlled and maintained. Fuel flowrate to the engine was measured using a Sierra CP gravimetric fuel balance system, at a frequency of 10 Hz. The closed-loop fuel control is realized via the engine control unit

(ECU). The test data were logged using a Sierra CP CADET Host control and acquisition system, at a frequency of 10 Hz.

Piston surface temperatures were measured in six locations over the piston crown of one instrumented piston, using fast response thermocouples with sensing elements of diameter 0.1 mm, located subsurface at a depth of 0.2 mm. Dong Yang telemetry technology was used to record the piston surface temperatures, this provided one reading every time the instrumented piston passed bottom dead center. These thermocouple data were recorded at 10 Hz with the other system measurements. The actual response time of the fast thermocouples in situ in the piston is not known precisely. However, the 10–90 response time for a thermocouple of around 0.1 mm size is of the order of 1 s or less, depending on the construction of the sensor [29]. Therefore, the rate of the measured temperature change is likely governed by the piston thermal inertia rather than the response time of the measurement system. The measured temperatures reported in this work were compared with measurements completed separately by the engine manufacturer prior to this work. These were performed on an engine of very similar design with a similarly instrumented piston. Good agreement was found for the PCJ off data, which could be directly compared.

A schematic representation of the thermocouples' locations is presented in Fig. 2. The thermocouple locations were identified prior to the PCJ experimental work using a combination of 3D CFD simulations of the fuel spray and in-cylinder images of the combustion [5]. The high-speed images were captured on another engine of the same design which was specially modified for endoscope access into one cylinder. A high-speed camera captured the fuel spray plume and combustion. Utilizing this combined information, thermocouples 3, 4, and 5 were selected to measure temperature in the area where CFD had predicted fuel spray impingement for one of the injection plumes. Thermocouples 2 and 6 were selected to characterize the temperature in adjacent nonimpingement locations; these two locations were also where the in-cylinder optical images had revealed diffusion flames were possible. Finally, thermocouple 1 was positioned between the valve recesses at the opposite side of the piston; this provided a reference temperature away from the fuel impingement zone.

Fig. 2 Schematic of thermocouples' locations on the piston crown surface
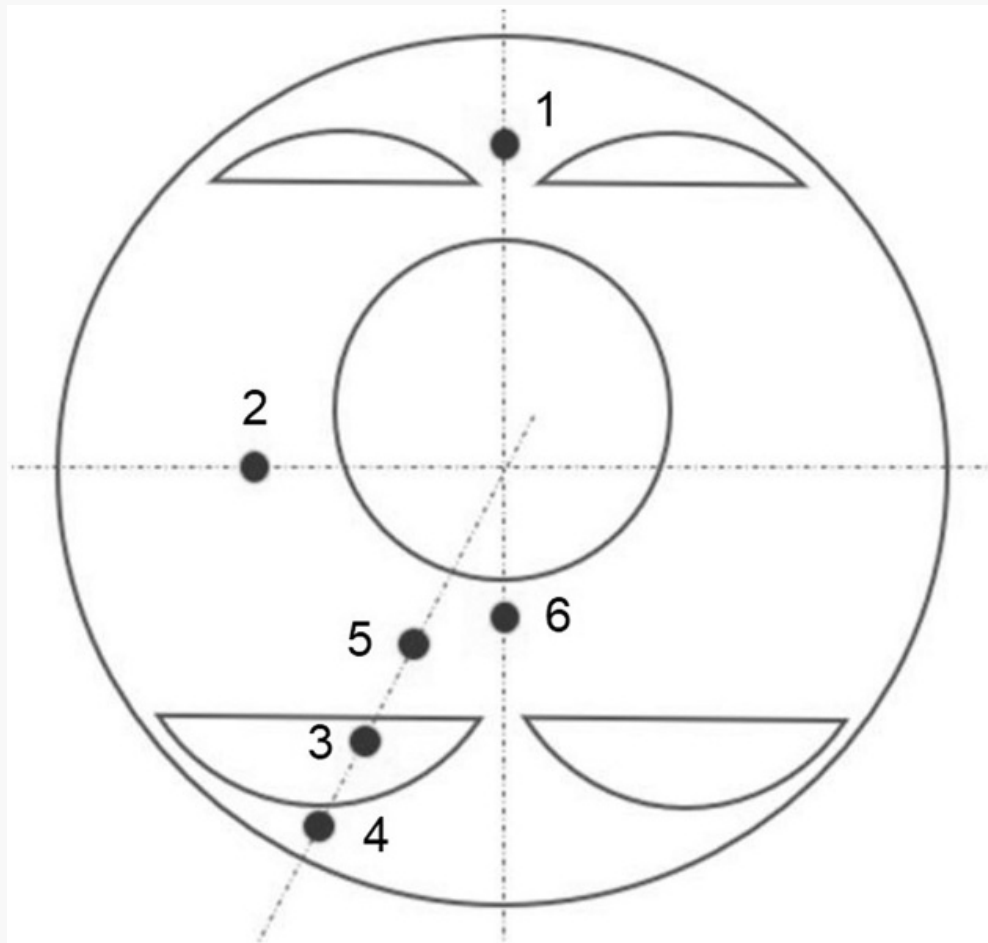
An average value for piston surface temperature was calculated from the six signals and used for the thermal modeling presented in this paper. Engine intake manifold, coolant, oil gallery (used for T_O), and exhaust manifold temperature were collected at a sample rate of 10 Hz, and used for model development and validation. The temperature in the exhaust manifold was measured using a thin, 0.1 mm fast-response sensing element. The measured mass air flow (MAF) rate of air into the engine was provided by the ECU. The ECU data were transferred to the CP Host system via ATI ASAP2 link with a sampling rate of 10 Hz.

Three types of engine tests were undertaken. The first type consists of steady-state engine running over a range of operating conditions with PCJ either on or off. Specifically, with PCJ off, data were collected at 14 operating conditions with engine speed in the range 1500–3000 rpm and torque in the range 20–100 Nm. These engine operating points were selected to cover the engine operating envelope where the impact of the

PCJ on piston temperature was of interest. The PCJ on/off state at each point was based on the normal engine control strategy for PCJ. At some points, the PCJ would be either on or off depending on certain decision variables in the strategy. This experimental design approach resulted in a somewhat smaller fraction of the experimental data being collected at the condition PCJ on versus PCJ off.

The steady-state test space is presented in Fig. 3. In all these tests, the engine was allowed to stabilize for at least 5 min to reach thermal equilibrium, before data recording. The tests were repeated several times across a number of days, providing slight variations of temperatures (and fuel consumption), which proved useful for model development and validation. The total number of steady-state data points with PCJ off and PCJ on was 53 and 15, respectively.

Fig. 3 Operating points for collection steady-state piston surface temperature with PCJ on/off
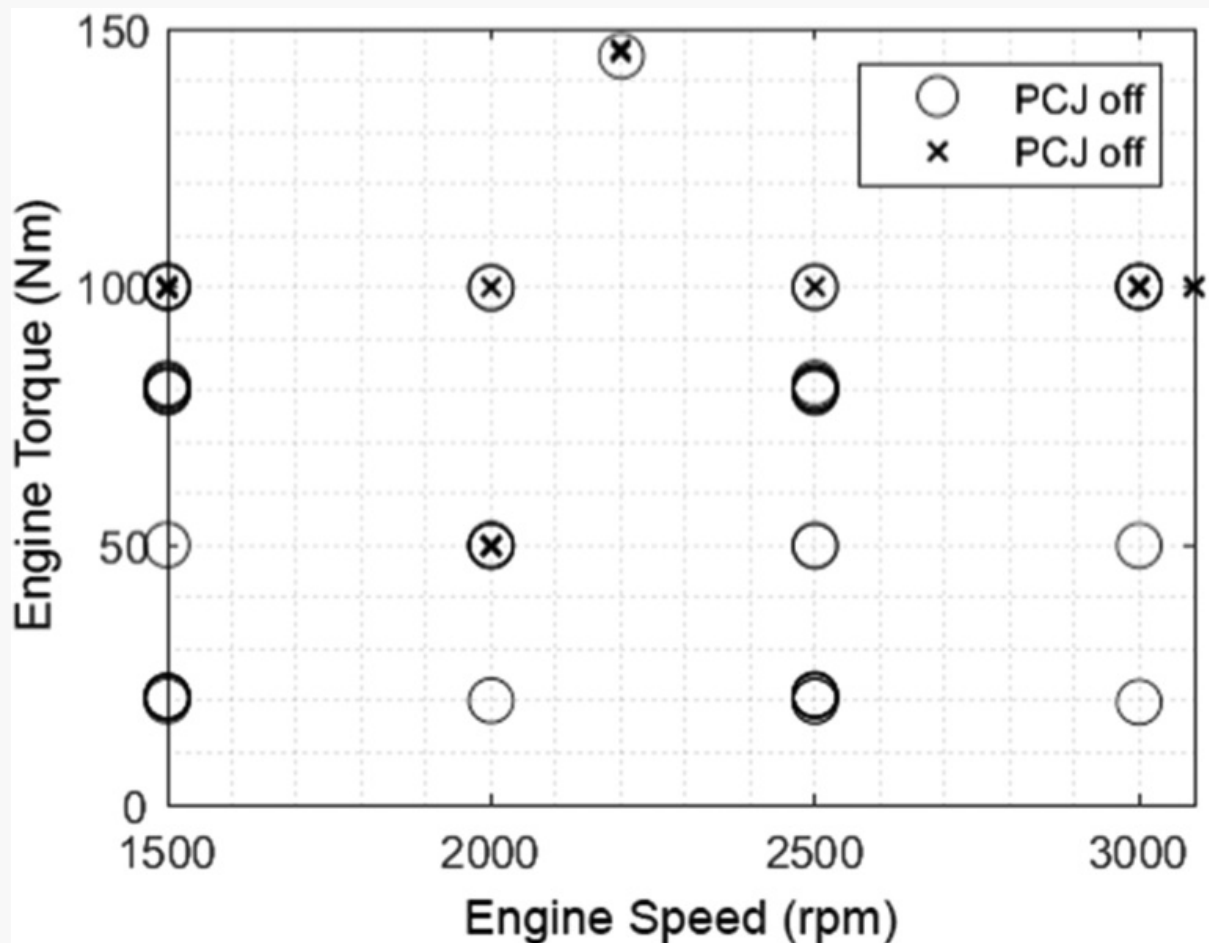
The second type of engine test was a transient torque ramp, where torque increased rapidly from 20 to 80 Nm

in 1 s, at two fixed levels of engine speed, 1500 and 2500 rpm. This is an increase in brake mean effective pressure from 2.52 bar to 10.07 bar. In these tests, the engine was allowed to reach steady thermal equilibrium before performing the torque ramp. The third type of test consisted of controlling the engine speed via the dynamometer to follow a chirp signal at constant torque. This test was used for model transient prediction validation.

All steady-state datasets and one torque ramp dataset (at 1500 rpm) were used for identification of the model parameters. The other ramp (at 2500 rpm) and the chirp transient dataset were used for model validation. Two extra datasets were also collected in separate tests and used for model validation. These consisted of constant speed-load PCJ off-on-off routines, where after thermal stabilization with PCJ off, the cooling jets were activated for 120 s, then de-activated once again. The first test was operated at 3000 rpm and 100 Nm, the second one at 1500 rpm and 100 Nm.

5 Model Performance

5.1 Model Performance for Training Data.

The first identified model parameter was η_h, which varies with the operating point in the engine speed and torque space. The results are shown in Fig. 4. The red stars are the locations of engine steady-state testing points (14 points). The surface was smoothed using a kernel regression model [30]. The same model is also used in the estimation of piston surface temperature in Eq. (25) and for computing $\dot{Q}_{cyl,1}$ in Eq. (28). From Fig. 4, it can be seen that the parameter η_h increases almost linearly as engine speed increases at fixed torque, the rate of change is more pronounced at lower torque (20 Nm) and less so at higher torque (100 Nm). No clear dependency is seen between η_h and engine torque.

Fig. 4 Identified Map for model parameter η_h
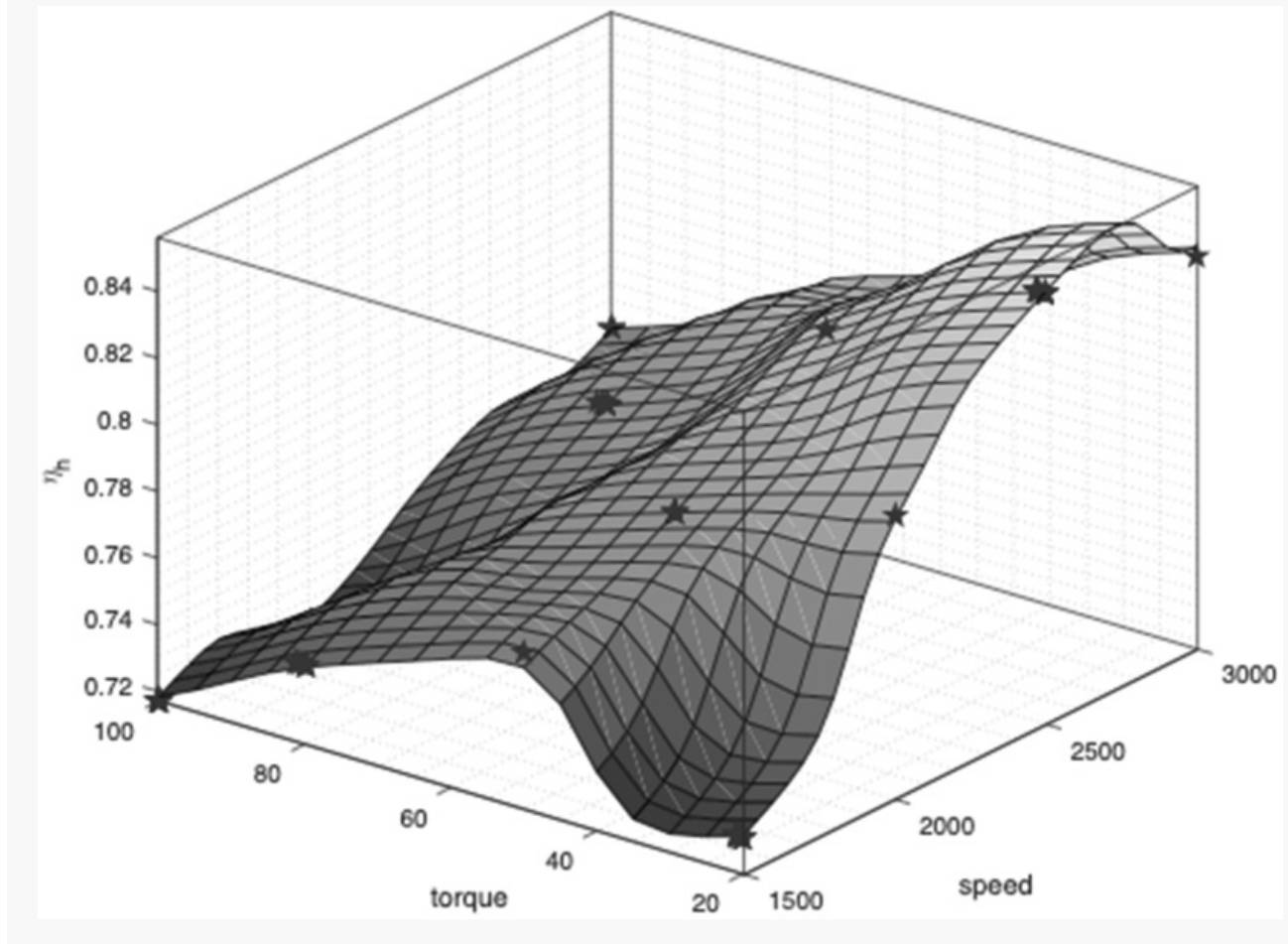
The four model constant parameters K_c, n_c, K_o, and n_o, identified through the steady-state engine data with both PCJ on and PCJ off, take the following values 20, 0.75, 19.2, and 0.77, respectively [31].

The modeled piston surface temperatures, plotted against the measured values, are shown in Fig. 5. The results show good agreement across the whole temperature range with an average accuracy of 1.2%. This is a very important first step for developing a good heat transfer model such as the one presented here.

Fig. 5 Modeled and measured piston surface temperature for steady-state operating conditions, with PCJ on and off (training data)
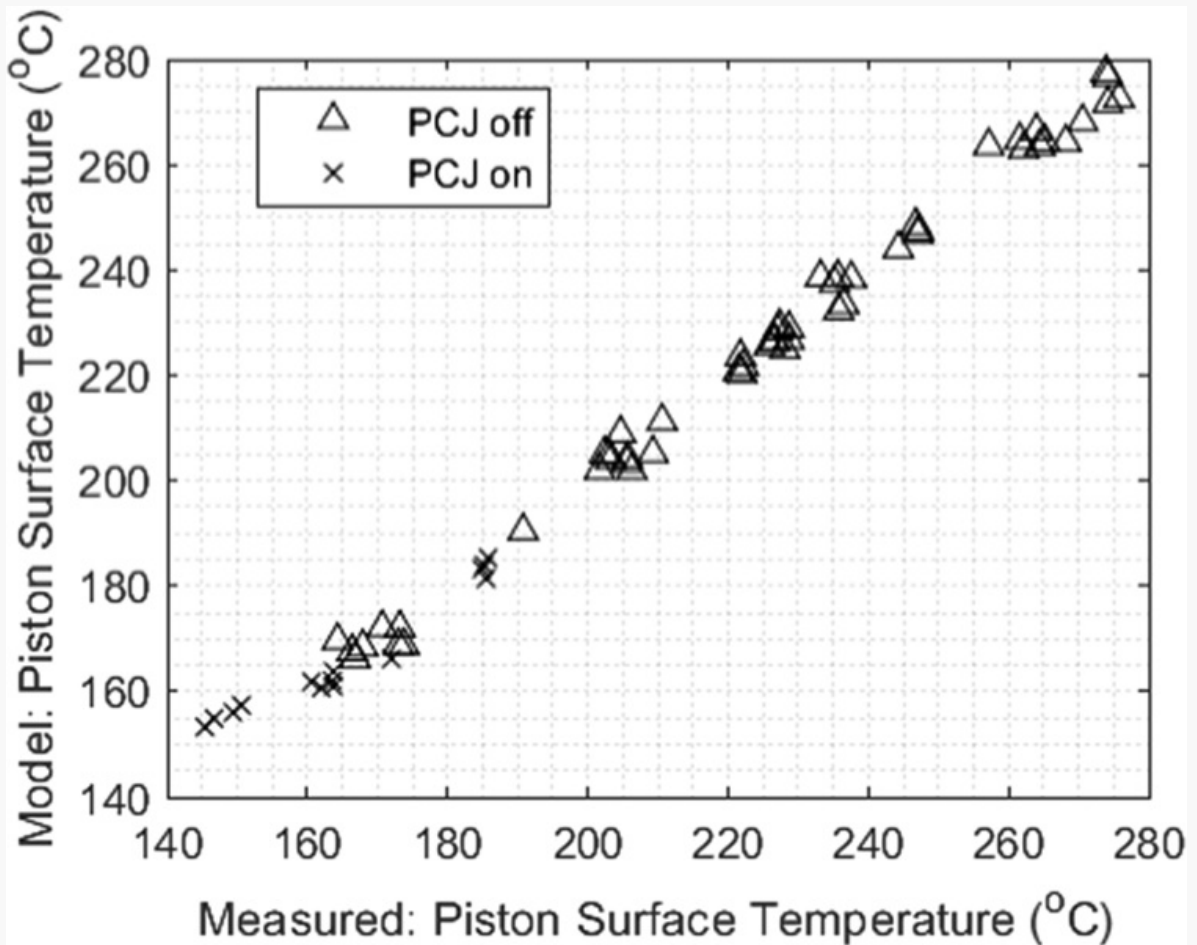
The first torque ramp transient test was used to identify the piston crown mass m_p, as described above using the optimization in Eq. (29). The identified piston mass was 3.06 kg (this is the combined mass of all three pistons). Modeled and measured piston surface temperatures for this transient test are shown in Fig. 6 as functions of elapsed test time. Considering the simplicity of the proposed model and the extremely complicated thermal dynamics involved in an ICE, these results also show good agreement. The calculated model accuracy across the torque/temperature ramp was between 0% and 4.53%, the average accuracy is 0.8%.

Fig. 6 Modeled and measured piston surface temperature for a rapid 1-s torque ramp between 20 and 80 Nm at constant speed of 1500 rpm (training data)
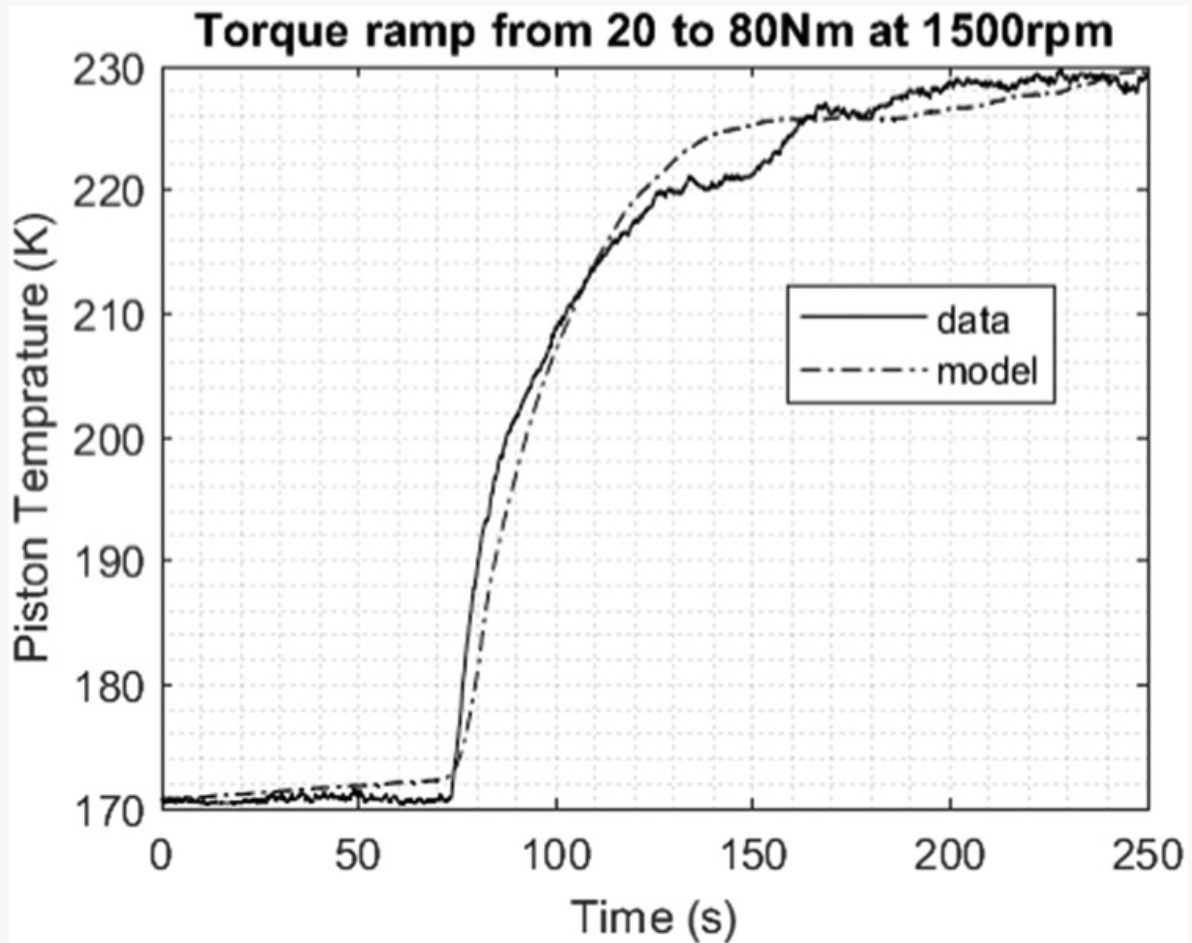
The thermal behavior of the piston top surface is noteworthy, and the potential implications rather significant. While the engine torque changes vary rapidly (1 s interval), the thermal inertia of the piston material causes a large delay in the temperature response. For the torque ramp shown in Fig. 6, the rapid temperature change interval spans 50 s approximately, from 75 to 125 s. As observed by Koepple [12], this thermal delay may be associated with large momentary particulate matter formation during transient engine operation (acceleration). This is similar to the effects of PCJ activation (off to on transition) as shown below by the results of the PCJ transient off-on-off routines, Figs. 7 and 8.

Fig. 7 Modeled and measured piston surface temperature during a PCJ off-on-off transient routine at 3000 rpm and 100 Nm (validation)
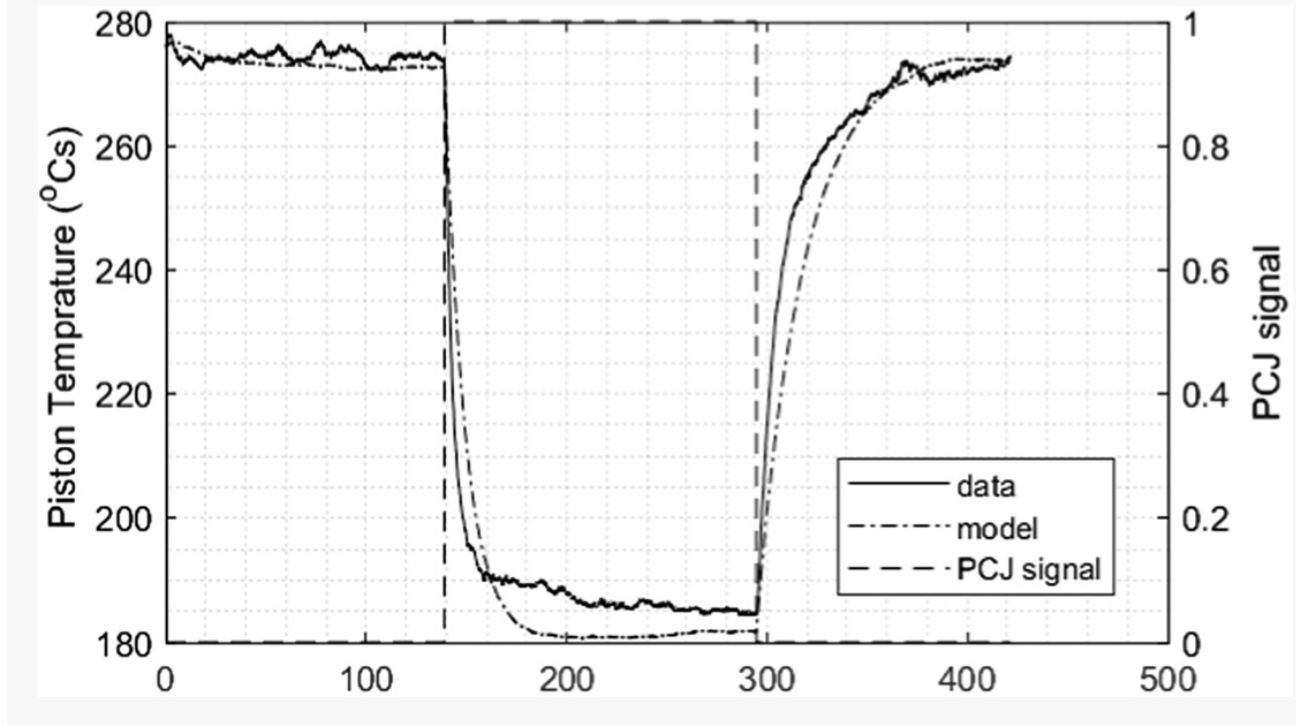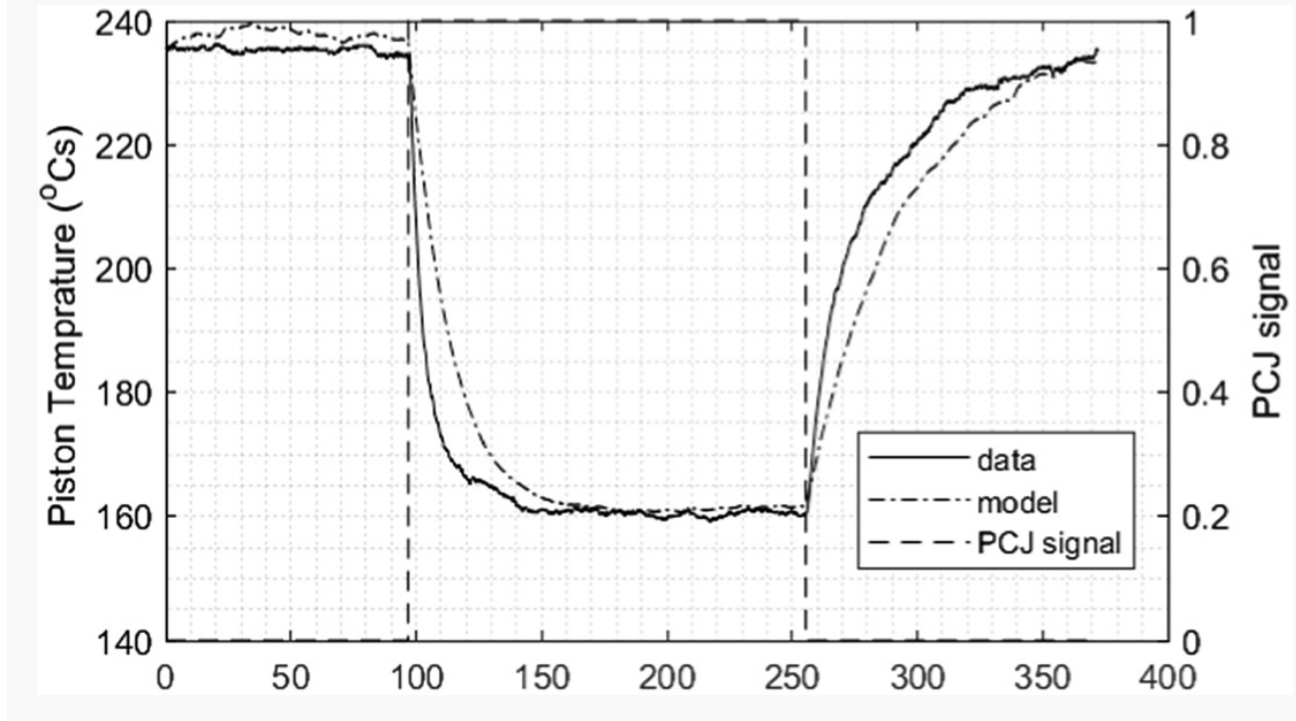
Fig. 8 Modeled and measured piston surface temperature during a PCJ off-on-off transient routine at 1500 rpm and 100 Nm (validation)

5.2 Model Performance for Validation Data.

The experimental data for the second torque transient ramp were used for model validation. The results are shown in Fig. 9. The accuracy of prediction for this validation exercise is good. The maximum model error is 2.5%. There is a discrepancy from 25 to 75 s between experimental and modeled data in Fig. 9. This is because this is validation data, not model training data. Hence, an extrapolated η_h value was used. The model error for this value might be the cause for this discrepancy.

Fig. 9 Modeled and measured piston surface temperature for a rapid 1-s torque ramp between 20 and 80 Nm at constant speed of 2500 rpm (validation data)
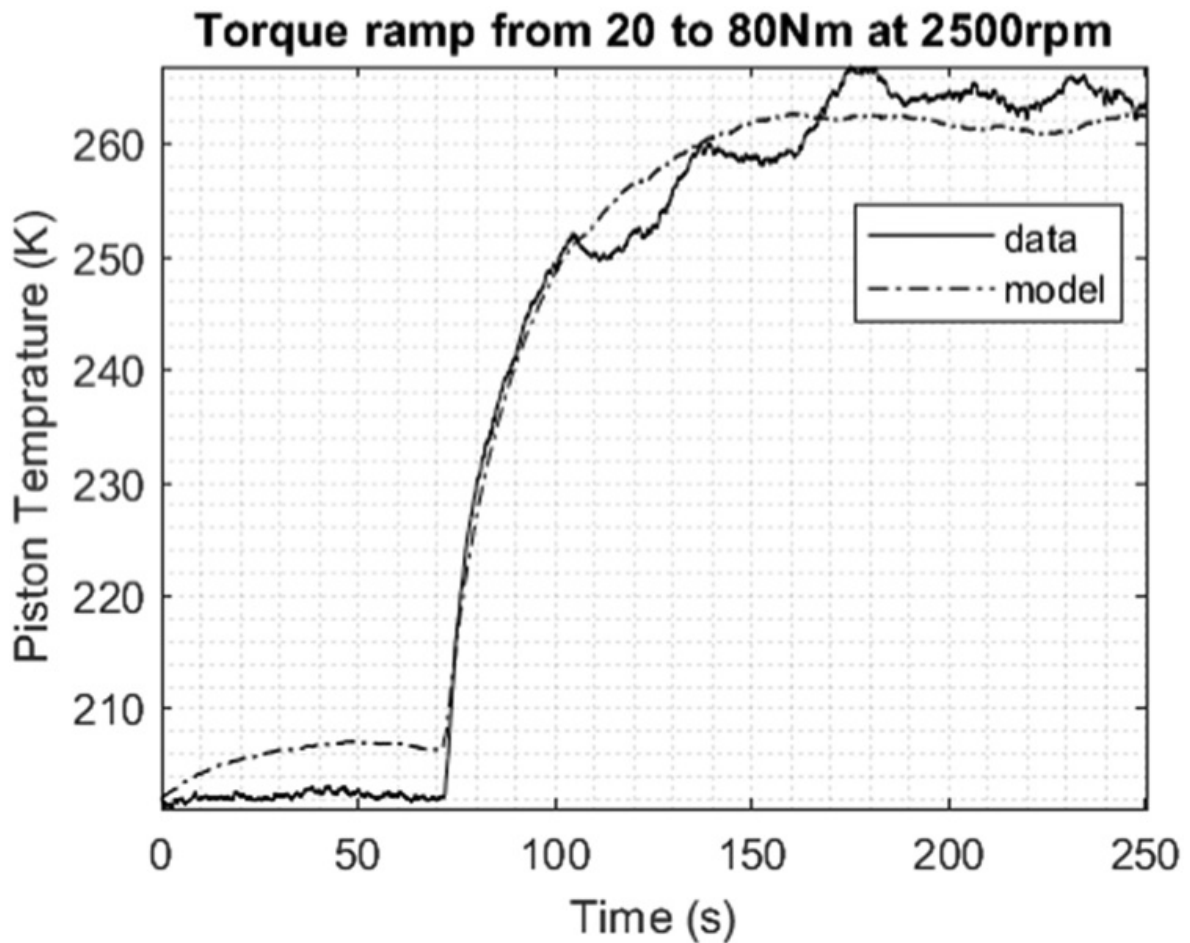
The proposed thermal model has also been validated against data from the PCJ off-on-off routines described above. The results are presented in Figs. 7 and 8, respectively, for the two chosen speed-load conditions. These figures, again, show good validation results. The model percentage average error for these two transient operations is 1.9% and 2.24%, respectively. This is good model performance for this highly transient thermal operation.

For completeness, Fig. 10 reports the experimental, time-resolved data for the ten relevant engine variables collected during the first PCJ transient routine. This is interesting as it shows that the extent to which the measured EXT and the oil temperature T_0 are both perturbed by enabling of the PCJ in the middle of the test sequence. The performance of the piston temperature model with these significant changes in the system is a

good indication of the model capability.

Fig. 10 Relevant engine variable signals acquired during the PCJ off-on-off transient routine at 3000 rpm and 100 Nm. The X-axes show time in seconds, the y-axes the variable and units reported on top of each plot
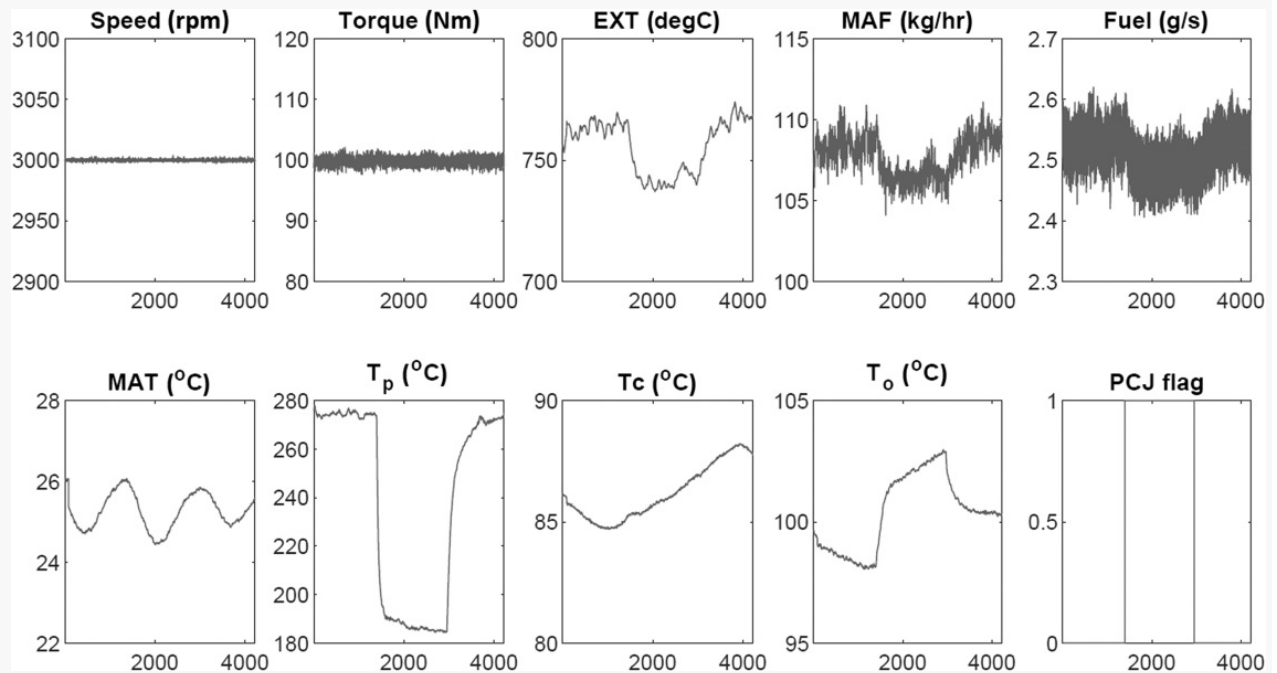

Figure 10 reveals that the fuel consumption rate, the MAF, and the exhaust temperature EXT all reduced slightly when the PCJ was on. This is intriguing as it indicates that the fuel was better utilized with PCJ on, improving the engine efficiency slightly at the same engine speed and torque. This could be from a reduction in frictional losses from the lower piston temperature. It could also be connected to differences in the oil system parasitic load on the engine with PCJ on/off. The lower wall temperatures may also decrease volumetric efficiency. As the engine in these experiments used closed-loop air–fuel ratio control, it likely some of the MAF change is from the engine control system adjusting the throttle for the slight reduction in fuel rate. Unfortunately, as cylinder pressure measurements were not available in these experiments, it is infeasible to identify the source(s) of this efficiency improvement. This is an interesting area for future work.

One further highly transient dataset was used for the validation of this piston surface temperature model. The engine speed was varied using a chirp signal; during the test, the PCJ was controlled by the engine control module. The engine speed, torque, PCJ flag, and other relevant signals for this test are reported in Fig. 11. This is a highly dynamic test with engine speed excitation frequencies and amplitudes, which are very severe versus normal operation.

Fig. 11 Engine variables during a chirp signal excited engine speed transient
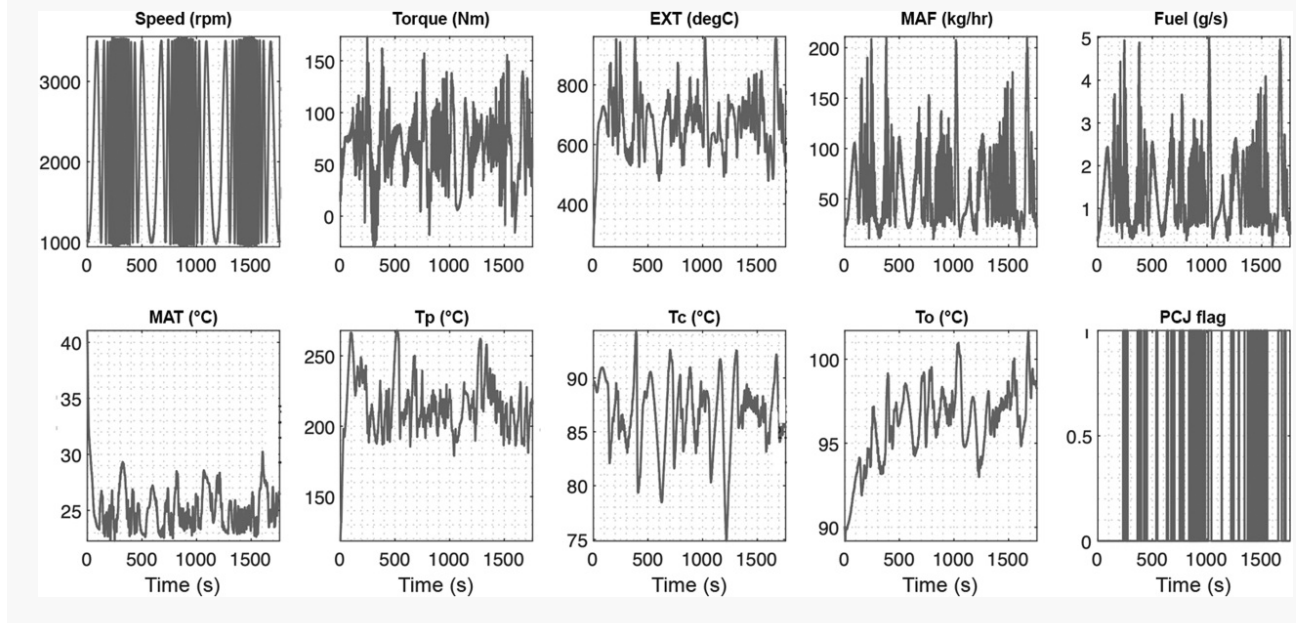
The piston surface temperature validation results are shown in Fig. 12, the average model accuracy is 6.68%. As the engine speed follows the chirp signal, the variation is high during the 200–300 s, 840 s–940 s, and 1420 s–1520 s intervals. The resulting model error is not considered poor, given that the exaggerated chirp condition is not expected during normal engine operation. The model performs well at predicting the overall piston temperature amplitude behavior between 180 and 280°C during this test. This model performance could be utilized for adaptive fuel injection and PCJ control strategies to help avoid fuel puddling on the piston crown.

Fig. 12 Model and measured piston surface temperature during chirp transient (validation data)
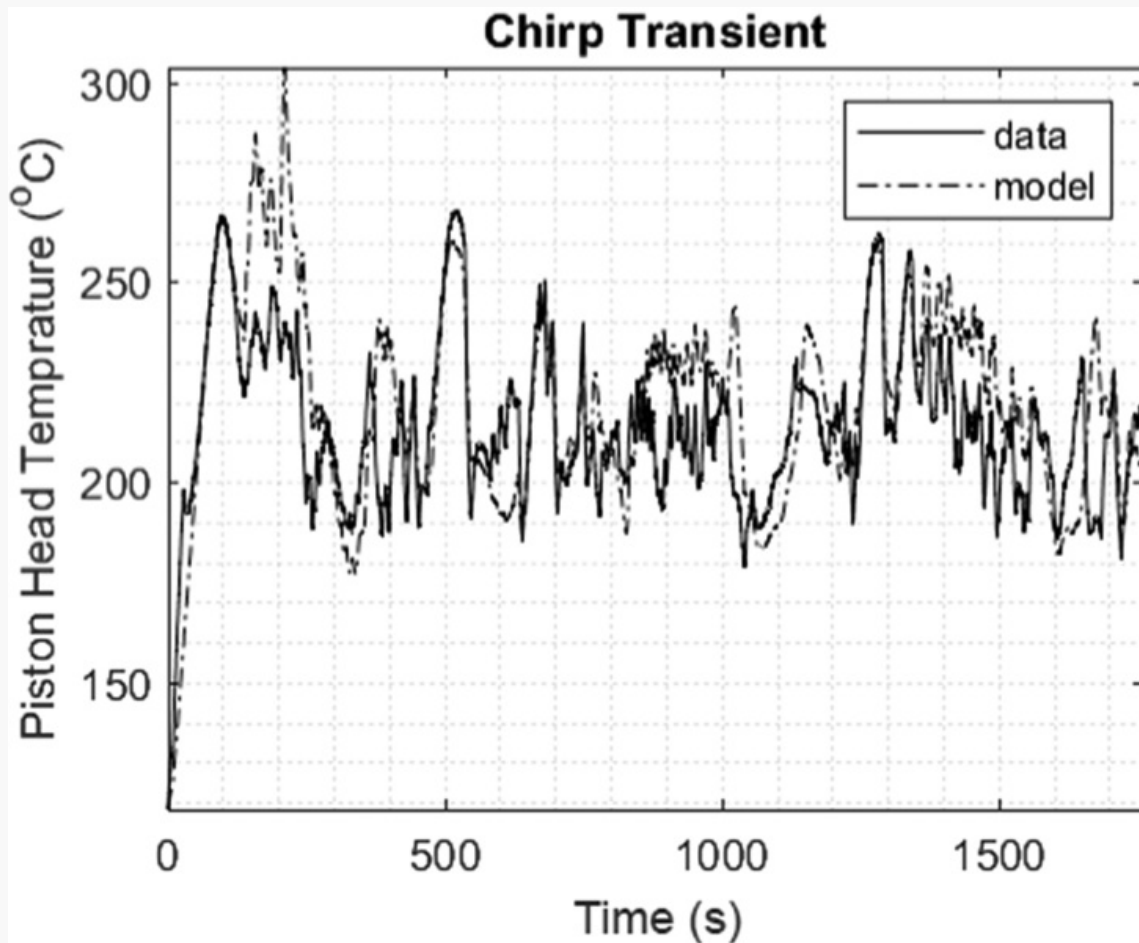
6 Conclusions

A dynamic model for estimating piston surface temperature has been developed in this paper. This model is distinctive for its accuracy and conciseness in predicting the piston surface temperature and the PCJ heat transfer effect inside the direct injection gasoline engine. The modeling approach is based on the external GEB principle. The model requires only nine measured variables as inputs that are straightforward to obtain from test data. The engine tests required for model parameter identification are PCJ on and off conditions at an engine steady-state and a single torque ramp test. Three optimization problems were formed and solved during the model parameter identification procedure. The model development process is much simpler compared to approaches found in the literature. This model provides sufficient prediction performance with average error of 6.68% during highly transient chirp input testing. The error is considerably lower during transients that are

more representative of real driving, e.g., 1.9–2.24%. The proposed model has potential to be utilized in adaptive multipulse fuel injection control strategies and also the control of PCJ systems; this could minimize the risk of fuel puddling on the piston crown during transient operation, which can help with minimizing harmful transient PN and HC emissions.

Funding Data

Data Availability Statement

The datasets generated and supporting the findings of this article are obtainable from the corresponding author upon reasonable request.

Nomenclature

A_p =

    cylinder reference area (m^2)

b =

    cylinder characteristic length, which normally refers to the cylinder bore (i.e. diameter) (m)

C_p =

    specific heat capacity of the piston crown (taken as 1020 $(\mathrm{J/kg \cdot K})$)

$C_{p,g}$ =

    gas specific heat capacity in $(\mathrm{kJ/kg \cdot K})$

h_c =

    overall heat transfer coefficient for coolant path $(\mathrm{W/m}^2/\mathrm{K})$

h_{cyl} =

    combustion overall heat transfer coefficient from piston surface to coolant and PCJ oil $(\mathrm{W/m}^2/\mathrm{K})$

h_{cyl} =

    heat transfer coefficient $(\mathrm{W/m}^2\mathrm{K})$

h_o =

    overall heat transfer coefficient for PCJ oil path $(\mathrm{W/m}^2/\mathrm{K})$

K =

    model constant (K_c - coolant path, K_o - PCJ oil jet path)

$k_g =$
gas thermal conductivity $(\mathrm{W/m \cdot K})$

$L =$
engine stroke length (m)

$\dot{m}_a =$
intake air mass flow rate $(\mathrm{kg/s})$

$\dot{m}_f =$
fuel mass flow rate $(\mathrm{kg/s})$

$m_p =$
lumped mass of the piston crown (kg)

$n =$
model power index constant (n_c - coolant path, n_o - PCJ oil jet path)

$N_e =$
engine rotational speed (rpm)

Nu =
Nusselt number (unitless)

$N_1 =$
total number of steady state data points with PCJ off

$N_2 =$
total number of steady state data points for PCJ on

$N_3 =$
total number of sample points within the torque ramp data set

$P_{\mathrm{out}} =$
engine mechanical brake power output (W)

$\dot{Q}_c =$
heat transfer rate from piston surface to coolant (W)

$\dot{Q}_{\mathrm{cyl,1}} =$
heat flow rate from hot combustion gas to piston surface (W)

$\dot{Q}_{\mathrm{cyl,2}} =$
heat transfer from combustion gas to coolant and to engine environment via ports and extra parts (other than piston crown) (W)

$\dot{Q}_{\mathrm{exh}} =$
heat transfer from the exhaust gas stream (W)

$\dot{Q}_{\mathrm{in}} =$
heat input from fuel (W)

$Q_{LHV} =$ lower heating value of the gasoline fuel (taken as 43.4 $(\mathrm{MJ/kg})$)

$\dot{Q}_o =$ heat transfer rate from piston surface to PCJ oil when PCJ is on (W)

$\dot{Q}_p =$ heat flow rate within the mass of the piston crown (W)

$r =$ model proportional term (0–1) to scale the heat input from fuel

$R_c =$ lumped thermal resistance: heat transfer path between piston surface and engine coolant $(\mathrm{K/W})$

$Re =$ Reynolds number (unitless)

$R_g =$ lumped thermal resistance: heat transfer path from the combustion gas to the piston surface $(\mathrm{K/W})$

$R_o =$ lumped thermal resistance: heat transfer path between piston surface and PCJ oil flowing within the piston crown $(\mathrm{K/W})$

$s_{PCJ} =$ denotes PCJ on and off (0 when PCJ is off, 1 when PCJ is on)

$T_c =$ coolant temperature (K)

$T_e =$ engine brake torque (Nm)

$T_{exh} =$ exhaust gas temperature (K)

$T_g =$ combustion gas temperature within cylinder $(^{\circ}\mathrm{C})$

$T_{in} =$ intake manifold temperature (K)

$T_o =$ oil jet temperature (K)

$T_p =$ measured piston surface temperature (K)

$\hat{T}_p =$ estimated piston surface temperature (K)

estimated piston surface temperature (K)

T_s =

sample time of the data collection during the experimental testing (s)

V_p =

mean piston speed $(\mathrm{m/s})$

η_c =

engine combustion efficiency (0–1)

η_h =

model identified parameter $(= (1-r)\eta_c)$

μ_g =

gas dynamic viscosity $(\mathrm{Ns/m^2})$

v_g =

gas kinematic viscosity $(\mathrm{m^2/s})$

Appendix A

A1 Gas Thermal Conductivity Two-Order Polynomial Regression Model.

k_g is the gas thermal conductivity with units of $(\mathrm{W/m \cdot K})$. Since it increases with temperature, a two-order polynomial regression model was used, as shown in Eq. (A1). This regression model was fitted using the air thermal conductivity data found in Ref. [28]

$$k_g = 10^{-3}(-0.0001T_g^2 + 0.068234T_g + 23.8) \tag{A1}$$

where T_g is the gas temperature within the cylinder, with units of $(^\circ\mathrm{C})$.

A2 Gas Dynamic Viscosity Two-Order Polynomial Regression Model.

μ_g is the gas dynamic viscosity, with units of $(\mathrm{Ns/m^2})$. The correlation with gas temperature, see Eq. (A2), was fitted using air dynamic viscosity data found in Ref. [28]

$$\mu_g = 10^{-6}(-0.000,013T_g^2 + 0.0435T_g + 17.222) \tag{A2}$$

A3 Gas Kinematic Viscosity Two-Order Polynomial Regression Model.

v_g is the gas kinematic viscosity, with units of $(\mathrm{m^2/s})$. A two-order polynomial regression model with respect to

gas temperature was used, Eq. (A3). This was obtained using air kinematic viscosity data found in Ref. [28]

$$\nu_g = 0.000,007 T_g^2 + 0.010,186,3 T_g + 1.3248$$ (A3)

A4 Gas-Specific Heat Capacity Fourth-Order Polynomial Regression Model.

$C_{p,g}$ is the gas specific heat capacity in $(\mathrm{kJ/kg \cdot K})$. As shown in Eq. (A4), it was fitted using a fourth-order polynomial equation correlated to gas temperature using air thermal conductivity data from Ref. [28]

$$\begin{aligned} C_{p,g} = &\ 2.2 \times 10^{-13}(T_g + 273.15)^4 - 8.92 \times 10^{-10} \\ &\ (T_g + 273.15)^3 + 1.234 \times 10^{-6}(T_g + 273.15)^2 \\ &\ - 4.8 \times 10^{-4}(T_g + 273.15) + 1.0595 \end{aligned}$$ (A4)

References

[1] Yan, F., and Wang, J., 2012, "Engine Cycle-by-Cycle Cylinder Wall Temperature Observer-Based Estimation Through Cylinder Pressure Signals," ASME J. Dyn. Syst., Meas., Control, 134(6), p. 061014.10.1115/1.4006222

[2] Wilhelmsson, C., Vressner, A., Tunestål, P., Johansson, B., Särner, G., and Aldén, M., 2005, "Combustion Chamber Wall Temperature Measurement and Modeling During Transient HCCI Operation," Powertrain and Fluid Systems Conference and Exhibition, SAE International, ▪San Antonio, Texas, ▪ October 24-27, 2005.

[3] Raza, M., Chen, L., Leach, F. C. P., and Ding, S., 2018, "A Review of Particulate Number (PN) Emissions From Gasoline Direct Injection (GDI) Engines and Their Control Techniques," Energies, 11(6), p. 1417.10.3390/en11061417

[4] United Nations for Economic Commission for Europe, 2019, ECE/TRANS/180/Add.15/Ammend.5, "Proposal for Amendment 5 to Global Technical Regulation No. 15 (Worldwide Harmonized Light Vehicles Test Procedures (WLTP))," United Nations.

[5] Biagiotti, F., Bonatesta, F., Tajdaran, S., Sciortino, D. D., Verma, S., Hopkins, E., Morrey, D., et al., 2022, "Modelling Liquid Film in Modern GDI Engines and the Impact on Particulate Matter Emissions - Part I," Int. J. Engine Res., 23(10), pp. 1634–1657.10.1177/14680874211024476

[6] Jiao, Q., and Reitz, R. D., 2015, "The Effect of Operating Parameters on Soot Emissions in GDI Engines," SAE Int. J. Engines, 8(3), pp. 1322–1333.10.4271/2015-01-1071

[7] Yusuf, A. A., and Inambao, F. L., 2019, "Effect of Cold Start Emissions From Gasoline-Fueled Engines of Light-Duty Vehicles at Low and High Ambient Temperatures: Recent Trends," Case Stud. Therm. Eng.,

14, p. 100417.10.1016/j.csite.2019.100417

[8] Pielaczyc, P., and Szczotka, A., 2011, "The Effect of Low Ambient Temperature on the Cold-Start Emissions and Fuel Consumption of Passenger Cars," SAE Int. J. Commer. Veh., 9(2), pp. 291–297.10.1177/0954407011406613

[9] Najafabadi, M. I., Mirsalim, M., Hosseini, V., and Alaviyoun, S., 2014, "Experimental and Numerical Study of Piston Thermal Management Using Piston Cooling Jet," J. Mech. Sci. Technol., 28(3), pp. 1079–1087.10.1007/s12206-013-1183-7

[10] Dhar, S., Godavarthi, R., Ranganathan, R., Mishra, A., and Bedekar, S., 2019, "A Transient, 3-Dimensional Multiphase CFD/Heat Transfer and Experimental Study of Oil Jet Cooled Engine P istons," WCX SAE World Congress Experience, SAE International, ▪Detroit, Michigan, ▪April 9-11. 2019.

[11] Luff, D. C., Law, T., Shayler, P. J., and Pegg, I., 2012, "The Effect of Piston Cooling Jets on Diesel Engine Piston Temperatures, Emissions and Fuel Consumption," SAE Int. J. Engines, 5(3), pp. 1300–1311.10.4271/2012-01-1212

[12] Kopple, F., Seboldt, D., Jochmann, P., Hettinger, A., Kufferath, A., and Bargende, M., 2014, "Experimental Investigation of Fuel Impingement and Spray-Cooling on the Piston of a GDI Engine Via Instantaneous Surface Temperature Measurements," SAE Int. J. Engines, 7(3), pp. 1178–1194.10.4271/2014-01-1447

[13] Kelleher, J., and Ajotikar, N., 2016, "Piston Cooling Nozzle Oil Jet Evaluation Using CFD and a High Speed Camera," SAE Int. J. Commer. Veh., 9(2), pp. 291–297.10.4271/2016-01-8100

[14] Chen, Y., Dhar, S., and Schlautman, J., 2020, "Experimental and Numerical Investigation of the Multiphase Flow and Heat Transfer in an Oil Jet Cooled Engine P iston," WCX SAE World Congress Experience, SAE International, ▪Detroit, Michigan, ▪April 21-23, 2020.

[15] Izadi, M., Hosseini, S. V., Alaviyoun, S. S., and Mirsalim, S. M. A., 2010, "Experimental and Numerical Analysis of the Piston Cooling Jet's Performance," ASME Paper No. ESDA2010-25145. 10.1115/ESDA2010-25145

[16] Kopple, F., Jochmann, P., Kufferath, A., and Bargende, M., 2013, "Investigation of the Parameters Influencing the Spray-Wall Interaction in a GDI Engine - Prerequisite for the Prediction of Particulate Emissions by Numerical Simulation," SAE Int. J. Engines, 6(2), pp. 911–925.10.4271/2013-01-1089

[17] Zheng, M., and Kumar, R., 2009, "Implementation of Multiple-Pulse Injection Strategies to Enhance the Homogeneity for Simultaneous Low-NO$_X$ and -Soot Diesel Combustion," Int. J. Therm. Sci., 48(9), pp. 1829–1841.10.1016/j.ijthermalsci.2009.02.009

[18] Yoshihiro, I., and Kiyotaka, S., 2015, "A Study of Multistage Injection Mechanism for Improving the Combustion AQ7 of Direct-Injection Gasoline Engine," SAE Int. J. Commer. Veh., 9(2), pp. 291–297.

[19] Woschni, G., 1967, "A Universally Applicable Equation for the Instantaneous Heat Transfer Coefficient in the Internal Combustion Engine," SAE Transactions, 76(4). pp. 3065-3083. 10.4271/670931.

[20] Chang, K., Lavoie, G. A., Babajimopoulos, A., Filipi, Z., and Assanis, D. N., 2007, "Control of a Multi-Cylinder HCCI Engine During Transient Operation by Modulating Residual Gas Fraction to Compensate for Wall Temperature Effects," SAE World Congress and Exhibition, SAE International, Detroit, Michigan, April 16-19, 2007.

[21] Yan, Z., Gainey, B., and Lawler, B., 2022, "A Parametric Modeling Study of Thermal Barrier Coatings in Low-Temperature Combustion Engines," Appl. Therm. Eng., 200(▪), p. 117687.10.1016/j.applthermaleng.2021.117687

[22] Yan, Z., Levi, A., Zhang, Y., Sellnau, M., Filipi, Z., and Lawler, B., 2023, "A Numerical Evaluation and Guideline for Thermal Barrier Coatings on Gasoline Compression Ignition Engines," Int. J. Engine Res., 24(5), pp. 2206–2222.10.1177/14680874221114534

[23] Gandolfo, J., Gainey, B., Yan, Z., Jiang, C., Kumar, R., Jordan, E. H., Filipi, Z., and Lawler, B., 2023, "Low Thermal Inertia Thermal Barrier Coatings for Spark Ignition Engines: An Experimental Study," Int. J. Engine Res., 24(7), pp. 3297–3313.10.1177/14680874221149458

[24] Payri, F., Olmeda, P., Martin, J., and Carreño, R., 2014, "A New Tool to Perform Global Energy Balances in DI Diesel Engines," SAE Int. J. Engines, 7(1), pp. 43–59.10.4271/2014-01-0665

[25] Benajes, J., Olmeda, P., Martín, J., Blanco-Caver, D., and Warey, A., 2017, "Evaluation of Swirl Effect on the Global Energy Balance of a HSDI Diesel Engine," Energy, 122(▪), pp. 168–181.10.1016/j.energy.2017.01.082

[26] Taylor, C. F., 1985, The Internal-Combustion Engine in Theory and Practice: Combustion, Fuels, Materials, Design, MIT Press, M.I.T. Press, Cambridge, Massachusetts.

[27] Fonseca, L., Olmeda, P., Novella, R., and Valle, R. M., 2020, "Internal Combustion Engine Heat Transfer and Wall Temperature Modeling: An Overview," Arch. Comput. Methods Eng., 27(5), pp. 1661–1679.10.1007/s11831-019-09361-9

[28] Ferguson, C., and Kirkpatrick, A., 2015, Internal Combustion Engines: Applied Thermosciences, Wiley, ▪Hoboken, New Jersey.

[29] OMEGA, 2024, "Thermocouple Response Time Information for Ultra-Fine Thermocouples," accessed Jan 29, 2024, https://www.omega.com/en-us/resources/thermocouples-response-time

[30] Blundell, R., and Duncan, A., 1998, "Kernel Regression in Empirical Microeconomics," J. Human Resour., 33(1), pp. 62–87.10.2307/146315

[31] Brown, R., and Hwang, P., 1997, Introduction to Random Signals and Applied Kalman Filtering, 3rd ed., Wiley, Hoboken, New Jersey.